

# Study of the Falling Friction Effect on Rolling Contact Parameters

Juan Giner<sup>1</sup> · Luis Baeza<sup>2</sup>  · Paloma Vila<sup>1</sup> · Asier Alonso<sup>3</sup>

Received: 21 March 2016 / Accepted: 31 December 2016 / Published online: 10 January 2017  
© The Author(s) 2017. This article is published with open access at Springerlink.com

**Abstract** The existence of a wheel–rail friction coefficient that depends on the slip velocity has been associated in the literature with important railway problems like the curving squeal and certain corrugation problems in rails. Rolling contact models that take into account this effect were carried out through the so-called Exact Theories adopting an exact elastic model of the solids in contact, and Simplified Theories which assume simplified elastic models such as Winkler. The former ones, based on Kalker’s Variational Theory, give rise to numerical problems; the latter ones need to adopt hypotheses that significantly deviate from actual conditions, leading to unrealistic solutions of the contact problem. In this paper, a methodology based on Kalker’s Variational Theory is presented, in which a local slip velocity-dependent friction law is considered. A formulation to get steady-state conditions of rolling contact by means of regularisation of the Coulomb’s law is proposed. The model allows establishing relationships in order to estimate the global properties (creepage velocities vs. total longitudinal forces) through local properties (local slip velocity vs. coefficient of friction) or vice versa. The proposed model shows a good agreement with experimental tests while solving the numerical problems previously mentioned.

**Keywords** Rolling contact · Falling friction coefficient · Coulomb’s law regularisation

## 1 Introduction

Rolling contact models are widely used in railway technology in order to compute wheel–rail contact forces or estimate wheel and rail wear. With few exceptions, these contact theories implement the original Coulomb’s law with a constant friction coefficient. Nevertheless, the existence of a coefficient of friction falling with the slip velocity has been associated (together with another mechanisms) with corrugation of rails [1], or squeal noise in narrow curves [2]. Figure 1 shows the creep force versus creepage when both a constant finite and an infinite friction coefficients are considered. The same plot presents the expected creep force when a falling friction coefficient is adopted, which is differentiated by a local minimum that would explain stick–slip phenomena.

Some researchers have developed rolling contact theories that represent the dependence of the coefficient of friction on the slip velocity, generally by two coefficients of friction (static/kinematic). These models are either Simplified Theories (see definition in [3], and examples in [4, 5]), that somehow simplify the relationships between the contact traction distributions and the displacements in the contact area, or they are based on the Kalker’s tangential Variational Theory [3], that introduces a half-space elastic model in the formulation (Exact Theory). The Simplified Theories are adjusted to converge to the results from the Exact Theories, giving a good agreement when comparing the velocity of the wheel–rail contact point (creepages) and forces [3]. However, this agreement does not occur for the local slip velocities [6] and consequently,

✉ Luis Baeza  
L.Baeza@soton.ac.uk

<sup>1</sup> Centro de Investigación en Ingeniería Mecánica, Universitat Politècnica de València, Camino de Vera s/n, 46022 Valencia, Spain

<sup>2</sup> Institute of Sound and Vibration Research, University of Southampton - Highfield, B13/R3075, Southampton SO17 1BJ, UK

<sup>3</sup> CAF I+D, José Miguel Iturrioz, 26, 20200 Beasain, Spain

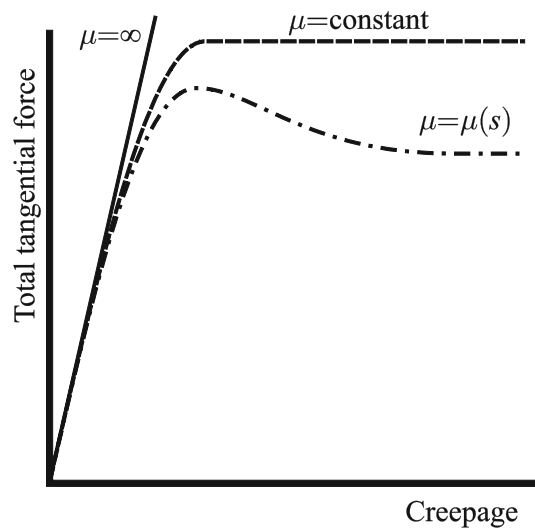


**Fig. 1** Behaviour of the creep force and local traction distribution depending on the friction coefficient:  $\mu = \infty$  (adhesion model),  $\mu = \text{constant}$  finite value, and  $\mu = \mu(s)$  as a function of the slip velocity  $s$

the high errors resulting in the slip velocities seem to make the Simplified Theories inadequate to model the contact process through a non-constant coefficient of friction that depend on the slip velocity.

Kalker's Variational Theory is potentially a good approach since it is based on realistic assumptions of the rolling contact problem and does not introduce unrealistic hypotheses as Simplified Theories do. Nevertheless, the computed contact traction distribution presents a saw-teeth shape [7–9], which is either considered as a reliable solution by some authors, or a numerical error. The implementation of the velocity-dependent friction coefficient makes the physics strongly nonlinear, and multiple solutions could satisfy the rolling contact problem equations.

In this paper, a methodology based on Kalker's Variational Theory is presented in which the falling friction coefficient is considered. The original instationary method is modified in order to obtain the steady-state solution of the rolling contact problem. The numerical problems found in the literature are solved through the implementation of the Coulomb's law regularisation. A methodology is proposed for relating the contact global properties associated with creepage velocities and total longitudinal forces, with local properties such as local slip velocity and dependent friction characteristics. These relationships avoid adopting incompatible contact parameter sets.

The present approach adopts experimental results published in [10] (see test-bench image in Fig. 2). The literature shows creep curves measured in real field experiments (see examples provided in [11, 12]) in order to study the locomotive traction capability. In such cases, the longitudinal creepage typically reaches values of 50% and higher,

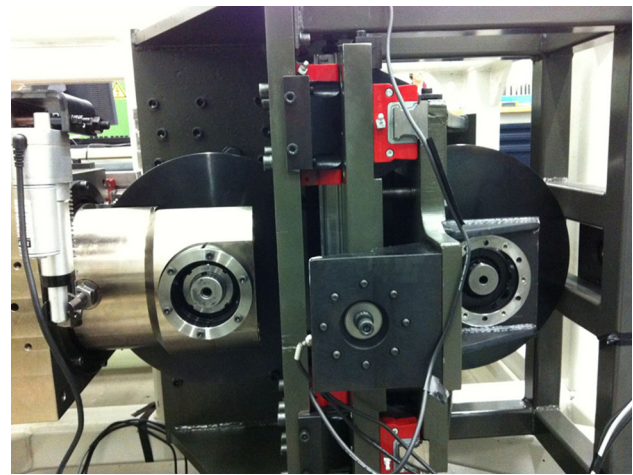


**Fig. 2** Rolling contact test-bench at CEIT

whereas the creepage is lower than 3% in most of the railway dynamic problems within the scope of the present paper.

Creep velocity is a phenomenon due to the displacements associated with the elastic deformations close to the contact area, and the local slip velocities, as it will be shown in Sect. 2. The Linear Contact Theory [13] neglects the local slip velocity (it is a so-called adhesion theory), and according to this theory the total force  $F_1$  is  $f_{11}\xi_1$ , being  $\xi_1$  the longitudinal creepage and  $f_{11}$  the creep (Kalker's) coefficient. The maximum longitudinal force per wheel in typical European networks rarely exceeds 50 kN, and a typical creep coefficient  $f_{11}$  is around  $1.5 \times 10^7$  N. If only the displacements associated with the elastic deformations would explain the creepage value, in this unfavourable scenario the creepage will be (through the Linear Theory equation) only 0.3%. Consequently, typical creepage values that are considered in locomotive traction tests are dominated by the slip velocity at the wheel–rail contact point, the full contact area is slip area, and the role of the displacements associated with the elastic deformations is negligible.

For low creepages, the creep–force relationship presents a high gradient and the possible accuracy of the creepage measurement in a real railway vehicle cannot permit to obtain good precision if the creepage is low. The needed accuracy is reached in the laboratory bench of Ref. [10] (with a 0.05% of error in creepage), for slightly larger creepages than the ones of the saturation conditions, which is the case of interest in the main problems in railway dynamics. The proposed approach tries to reproduce these experimental results where the displacements associated with the elastic deformations must be considered in the physical model.

The model adopted in this work is presented in Sect. 2 of this paper. In order to present parameters and establish

the formulation, this section summarises the Kalker’s Variational Theory which is extensively explained in [3, 14]. Implementing a falling friction coefficient model, the formulation introduces local parameters that define the friction coefficient as a function of the slip velocity. These parameters are also related with the global parameters that characterise the creep curves (tangential forces vs. creepages). The formulae that relate the parameters of the rolling contact theory are presented in Sect. 3 of the present work. Section 4 of this article shows results from the proposed methodology.

## 2 Tangential Contact Model

An inertial reference system  $\mathbf{X}_1\mathbf{X}_2\mathbf{X}_3$  moving with the contact is adopted. The origin of the system is the theoretical contact point (point where the solids would be in contact if both were rigid). The  $\mathbf{X}_1$ -axis refers to the rolling (or longitudinal) direction and the  $\mathbf{X}_2$ -axis is associated with the lateral direction in such a way that  $\mathbf{X}_1\mathbf{X}_2$  is the tangential contact plane.

Kalker [3] deduced a kinematic model of the tangential contact that permits to relate the global displacement from the deformed and non-deformed configuration displacements. In this relationship, the velocity of the solids in contact can be described through the movement of the rigid solid and the displacements associated with the deformations as

$$\mathbf{s} = \mathbf{w} + 2 \frac{D\mathbf{u}}{Dt} = \mathbf{w} + 2 \frac{\partial \mathbf{u}}{\partial t} + 2V \frac{\partial \mathbf{u}}{\partial x_1}, \tag{1}$$

in which  $\mathbf{u}$  are the displacements associated with the elastic deformation of the solids in contact,  $\mathbf{s}$  is the local slip velocity,  $\mathbf{w}$  is the velocity associated with the undeformed configuration,  $V$  is the rolling velocity and  $D/Dt$  denotes the material derivative with respect to time. Vectors  $\mathbf{u}$ ,  $\mathbf{s}$  and  $\mathbf{w}$  are in the  $\mathbf{X}_1\mathbf{X}_2$  contact plane (they contain longitudinal and lateral components), and they are functions of the point  $\mathbf{x} = \{x_1, x_2\}^T$  within the contact area. Vector  $\mathbf{w}$  is obtained from the creepages as follows

$$\mathbf{w} = V \begin{Bmatrix} \xi_1 - x_2 \xi_{sp} \\ \xi_2 + x_1 \xi_{sp} \end{Bmatrix}, \tag{2}$$

where  $\xi_1$ ,  $\xi_2$  and  $\xi_{sp}$  are the longitudinal, lateral and spin creepages, respectively. The creepages  $\xi_1$  and  $\xi_2$  are computed as the velocities of the wheel contact point in the longitudinal and the lateral directions, respectively, divided by the rolling velocity. The creepage  $\xi_{sp}$  is the spin velocity (scalar product of the angular velocity of the wheel and the unit vector that is normal to the contact) divided by the rolling velocity. Assuming linear elastic behaviour of the

bodies in contact, the constitutive equation can be written as follows

$$\mathbf{u}(\mathbf{x}) = \int_S \mathbf{a}(\mathbf{x}, \mathbf{y}) p_1(\mathbf{y}) ds(\mathbf{y}) + \int_S \mathbf{b}(\mathbf{x}, \mathbf{y}) p_2(\mathbf{y}) ds(\mathbf{y}), \tag{3}$$

where the integral is extended to the contact surface.  $p_1$  and  $p_2$  are the longitudinal and lateral tractions, and vectors  $\mathbf{a}(\mathbf{x}, \mathbf{y})$  and  $\mathbf{b}(\mathbf{x}, \mathbf{y})$  contain the elastic influence functions. Integrals in Eq. (3) are the Boussinesq-Cerruti integrals when the elastic half-space hypothesis is adopted.

If the steady-state conditions are imposed, the partial derivative with respect to  $t$  in Eq. (1) is zero. By introducing the constitutive formula (3) in Eq. (1) and assuming steady-state response, this term results

$$\mathbf{s} = \mathbf{w} + 2V \int_S \left( \frac{\partial \mathbf{a}(\mathbf{x}, \mathbf{y})}{\partial x_1} p_1(\mathbf{y}) + \frac{\partial \mathbf{b}(\mathbf{x}, \mathbf{y})}{\partial x_1} p_2(\mathbf{y}) + \mathbf{a}(\mathbf{x}, \mathbf{y}) \frac{\partial p_1(\mathbf{y})}{\partial x_1} + \mathbf{b}(\mathbf{x}, \mathbf{y}) \frac{\partial p_2(\mathbf{y})}{\partial x_1} \right) ds(\mathbf{y}). \tag{4}$$

It must be pointed out that  $\mathbf{y}$  is the variable of integration in Eq. (4) and consequently it is independent of  $x_1$ . Therefore, the derivatives  $\partial p_1(\mathbf{y})/\partial x_1$  and  $\partial p_2(\mathbf{y})/\partial x_1$  are zero. Thus, Eq. (4) results

$$\mathbf{s} = \mathbf{w} + 2V \int_S \left( \frac{\partial \mathbf{a}(\mathbf{x}, \mathbf{y})}{\partial x_1} p_1(\mathbf{y}) + \frac{\partial \mathbf{b}(\mathbf{x}, \mathbf{y})}{\partial x_1} p_2(\mathbf{y}) \right) ds(\mathbf{y}). \tag{5}$$

The numerical resolution associated with Kalker’s tangential Variational Theory proposes a discretisation of the contact area into a regular mesh through rectangular elements, where the contact parameters are supposed constant. Let  $\mathbf{s}^J$ ,  $\mathbf{w}^J$  and  $\mathbf{p}^J$  be the parameters at the  $J$ th element. By considering the discretisation, Eq. (5) results

$$\mathbf{s}^J = \mathbf{w}^J + 2V \sum_{l=1}^N \left( p_1^l \int_{S^l} \frac{\partial \mathbf{a}(\mathbf{x}, \mathbf{y})}{\partial x_1} ds(\mathbf{y}) + p_2^l \int_{S^l} \frac{\partial \mathbf{b}(\mathbf{x}, \mathbf{y})}{\partial x_1} ds(\mathbf{y}) \right), \tag{6}$$

where  $N$  is the number of elements in the mesh and  $S^l$  is the contact surface of the  $l$ th element. By assuming half-space elastic behaviour of the solids, a closed-form solution of the integrals in Eq. (6) can be obtained. The corresponding integrals can be arranged in a matrix, giving

$$\mathbf{s}^J = \mathbf{w}^J + 2V \mathbf{C}^J \mathbf{p}, \tag{7}$$

where column matrix  $\mathbf{p}$  contains the tractions of the elements.

The original Kalker’s method needs to establish in Eq. (7) the elements of the mesh that are in adhesion and

those that are slipping. An alternative procedure is based on the regularisation of the Coulomb’s law, where the local traction distribution is formulated from the local slip velocities through a smooth fitting function. The one adopted in this work is the following

$$p_{\kappa}^J \approx -\frac{2}{\pi} \arctan\left(\frac{\|s^J\|}{\varepsilon}\right) \frac{\mu p_3^J s_{\kappa}^J}{\|s^J\|}, \quad \kappa = 1, 2, \tag{8}$$

with  $\mu$  being the friction coefficient. The formula of Eq. (8) converges to the Coulomb’s law when  $\varepsilon$  approaches zero. The parameter  $\varepsilon$  must be chosen small enough such that the error of the regularisation is minimised, but the convergence to the solution is compromised if  $\varepsilon$  is too small. The present work adopts  $\varepsilon = 10^{-8}$  m/s, which allows obtaining results in agreement with the original Coulomb’s law.

The regularisation of the Coulomb’s law has the following advantages. Firstly, the unknowns in the rolling contact equation Eq. (8) are reduced to local slip velocities, and the computational cost is smaller since the iterative process of the original Variational Theory (where sets of adhesion and slip elements are tested) is avoided. Secondly, it facilitates to implement a friction coefficient  $\mu$  that depends on the local slip velocity. And finally, all the contact parameters are smooth distributions even in the border between the adhesion/slip areas.

An exponential falling model for the local slip velocity-dependent friction coefficient is chosen in the present work since it is widely used in the literature as a simplification of the Stribeck’s friction law [15], without considering the hydrodynamic ascending regime for high slip velocities. Based on the experimental results from [10], in which the total tangential force is stabilised for high creepages, a constant kinematic friction coefficient was taken into account, giving the following formula

$$\mu(s) = \mu_k + (\mu_s - \mu_k) e^{-c_{\mu}\|s\|}, \tag{9}$$

where  $\mu_s$  and  $\mu_k$  are the static and the kinematic friction coefficients, respectively, and  $c_{\mu}$  is an exponential parameter.

**Fig. 3** Different friction coefficient models. *Continuous trace* falling friction coefficient through Eq. (9), being  $\mu_s = 0.45$ ,  $\mu_k = 0.4$  and  $c_{\mu} = 1.15 \times 10^4$  s/m. *Dashed trace* regularisation of Coulomb’s law with constant friction coefficient  $\mu = 0.4$ . *Dotted trace* regularisation of Coulomb’s law where the friction coefficient follows Eq. (9)

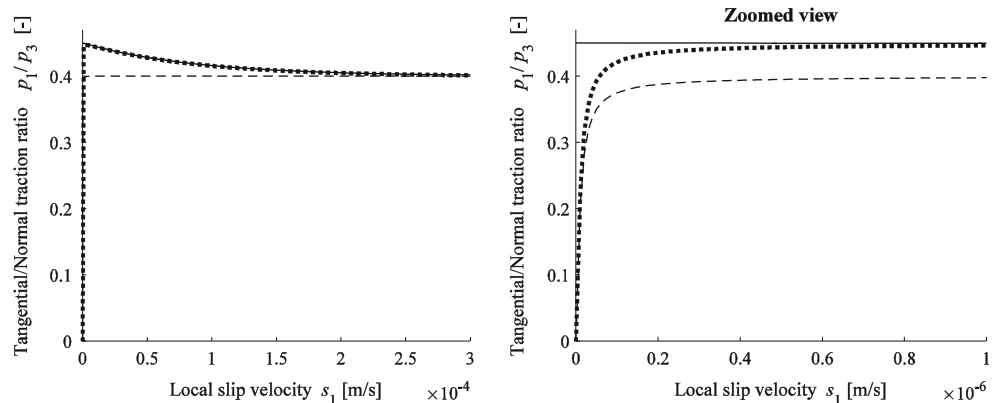


Figure 3 shows three models of the friction coefficient. The right plot is a zoomed view of the left one. The figure represents the total tangential traction versus normal traction curves through different approaches. In continuous trace, the curve represents a typical falling friction coefficient following Eq. (9). The other curves adopt regularisation by means of Eq. (8), and they present differentiable functions with a high gradient close to zero slip velocity. In dashed trace, the regularisation adopts a constant friction coefficient; in dotted line, it takes the former falling friction coefficient model.

### 3 Parameters of the Rolling Contact Model

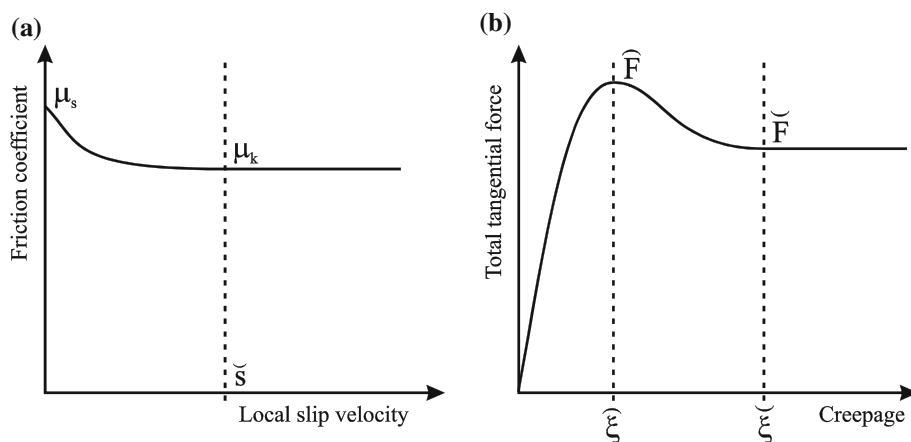
Figure 4 schematises the main relationships that involve the tangential rolling contact problem. On the left, Fig. 4a shows a model of the local slip velocity dependence of the friction coefficient. This model is associated with the local parameters of the wheel–rail contact, corresponding to Eq. (9); the static,  $\mu_s$ , and the kinematic,  $\mu_k$ , friction coefficients are introduced in that equation, together with the local slip velocity for which a value 1% above the kinematic friction coefficient,  $\tilde{s}$ , as follows

$$\mu(\tilde{s}) = \mu_k + 0.01 (\mu_s - \mu_k). \tag{10}$$

Figure 4b sketches the tangential contact relationship of the global parameters, following the results proposed in [16] for the rolling contact in the presence of a falling friction coefficient. The creep–total force curve presents a maximum of the contact force at the force–creepage pair  $(\tilde{F}, \tilde{\xi})$ . The total tangential force saturates at  $\tilde{F}$  for large creepage values, and the creepage from which this happens is  $\tilde{\xi}$ .

A mathematical relationship between the local parameters  $(\mu_s, \mu_k, \tilde{s})$  and creep parameters  $(\tilde{F}, \tilde{F}, \tilde{\xi}, \tilde{\xi})$  can be

**Fig. 4** Sketch of global and local parameters of the wheel–rail contact



revealed from the relationship between local slip velocity and contact tractions for steady-state condition in Eq. (7). This would permit to set the local parameters of the present tangential contact model from any experimental creep–total force curve in order to reproduce the behaviour of the contact forces in global terms from a physical model evaluated locally in every contour element of the mesh covering the contact area.

The saturation force  $\tilde{F}$  is obtained when the actual friction coefficient is  $\mu_k$  for all the elements of the mesh, that is

$$\tilde{F} = \mu_k \sum_{J=1}^N a^J p_3^J, \tag{11}$$

where  $a^J$  is the area of the  $J$ th element.

Let us consider the case where the total force is  $\tilde{F}$  and the creepage is  $\tilde{\xi}$ . This case is reached when there is just one element where the local slip velocity is  $\tilde{s}$  (the other elements have  $\|s^J\| \geq \tilde{s}$ ). This element must be at the leading edge of the contact area. Without loss of generality, let us consider a 2-dimensional contact case, where the element at the leading position is numbered as  $L$ . Equation (7) can be written for the present case as follows

$$s_1^L = \tilde{s} = V\tilde{\xi} + 2V \sum_i C_{1i}^L \mu_k p_3^i, \tag{12}$$

It must be pointed out that the friction coefficient model associated with Eq. (12) does not attain the precise kinetic value  $\mu_k$ . The kinetic friction coefficient  $\mu_k$  is assumed to be  $\mu(\tilde{s})$ , obtaining the following constrain equation

$$\tilde{s} = V\tilde{\xi} + 2V \sum_i C_{1i}^L \mu(\tilde{s}) p_3^i. \tag{13}$$

The peak force  $\hat{F}$  and the creepage  $\hat{\xi}$  are related through the following equation

$$\left. \frac{\partial F}{\partial \xi} \right|_{\hat{F}, \hat{\xi}} = 0. \tag{14}$$

The derivative of Eq. (14) can be obtained by means of finite differences. Equations (9), (13) and (14) constrain the values of the local parameters  $(\mu_s, \mu_k, \tilde{s})$  and the global parameters  $(\hat{F}, \tilde{F}, \hat{\xi}, \tilde{\xi})$ . Consequently, no more than four parameters can be set. Hence, these equations permit to make a reliable approach for the local parameters that characterise the tangential contact model from the global parameters extracted from any experimental creep curve.  $\mu_s, \mu_k$  are needed for the definition of the falling friction coefficient in Eq. (9), and  $\tilde{s}$  permits to evaluate the exponential  $c_\mu$  used in this equation from Eq. (10):

$$c_\mu = -\frac{\log(0.01)}{\tilde{s}}. \tag{15}$$

## 4 Results

### 4.1 First Analysis Through a 2D Approach

In this section, results from calculations performed using the proposed model are presented. The approach is limited to a 2-dimensional case. This restrictive hypothesis permits to compare with Carter’s model [17], which provides an analytical reference solution of the 2D case. For the studied case, the solids in contact are considered cylindrical. The material (a type of rubber much softer than steel) and the geometrical properties together with the model parameters are detailed in Table 1.

The first result is shown in Fig. 5 where the contact traction distribution is plotted for  $\mu_k = 0.35$  and  $\mu_s = 0.45$ . The same calculation is carried out through three different approaches. One of them was the Carter’s model with a



**Table 1** Parameters of the model

Shear modulus, $G$ (N/m <sup>2</sup> )	$1.0 \times 10^6$
Poisson's ratio, $\nu$ (-)	0.28
Roller 1 radius, $r_{11}$ (mm)	337.5
Roller 2 radius, $r_{21}$ (mm)	337.5
Normal contact force, $F_3$ (N)	470.5
Vehicle speed, $V$ (m/s)	25
Number of elements in spatial discretisation, $N$	100
Local slip saturation value, $\bar{s}$ (m/s)	0.2

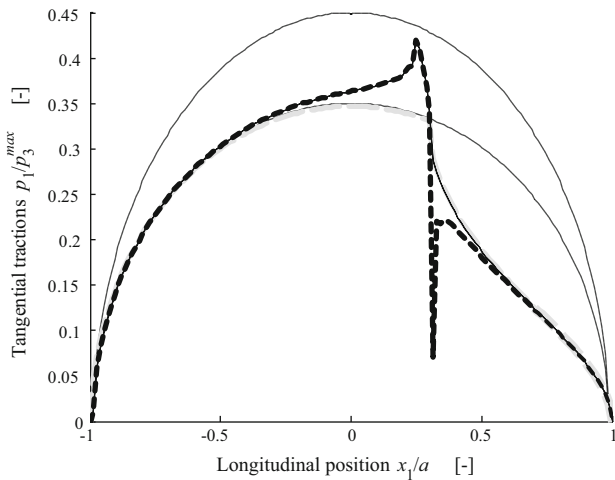


**Fig. 5** Tangential traction distribution for falling exponential coefficient of friction. *Thin solid line* static and kinematic bounds; *grey rectangles* Carter's analytical solution; *filled squares* numerical solution without regularisation; *thick solid line* numerical solution with regularisation

single friction coefficient  $\mu_k$ . The other approaches consist in the Kalker's Variational Theory with and without regularisation, where the friction coefficient is introduced through the model proposed in Eq. (8). Figure 5 also shows the bound limits established by the kinematic and the static friction coefficients.

The model that adopts regularisation and the Carter's model produce indistinguishable results in the Carter's adhesion area, whereas the Variational Theory leads to the same results in the Carter's slip area. Both approaches induce a peak in the slip-adhesion border, as a consequence of the decreasing friction coefficient.

The tangential traction distribution obtained using the Variational Theory without regularisation presents a dip in the adhesion area that can be attributed to the numerical errors introduced by the discontinuity between the adhesion and the slip regions. Hence, regularisation permits to avoid that discontinuity in the equations, removing the dip as observed in Fig. 5. Thus, the transition is smooth, matching perfectly with the Carter's solution for the adhesion region.

Once introduced the regularisation, the work is focused on studying the effect of adopting two different coefficients of friction on the creep-force curves. Figure 6 presents different creep curves for a fixed value 0.30 of the kinematic coefficient and increasing values of the static coefficient. The tangential tractions are normalised by the normal load; thus, the saturation value of all the curves matches  $\mu_k$ . As shown in this figure, when both kinematic and static values are the same (constant coefficient of friction), the creep curve reproduces the expected behaviour reported in the literature, which serves as a base for Simplified Theories. When increasing the static value, a maximum appears around the creepage value of 0.01.

Following with the sensitivity study, the static value is set now to 0.45 and the kinematic one increases from 0.30 to 0.45. As expected, Fig. 7 shows that the maximum is more pronounced for higher differences between static and kinematic coefficients. Two observations must be highlighted: firstly, higher values of  $\mu_k$  displace the maximum to higher creepages; secondly, for a fixed  $\mu_s$ , the higher the fall in the friction law is considered (lower  $\mu_k$ ), the sooner and more pronounced will be the reduction of the initial slope of the creep curve.

The dependence of creep curves on vehicle velocity  $V$  is depicted in Fig. 8, where the total force is lower for intermediate creepages when increasing velocity. Thus, the magnitude of the maximum decreases for higher velocities, reaching the saturation value earlier.

Figures 9, 10 and 11 summarise the behaviour of previous curves depicting the normalised difference between the maximum longitudinal force with respect to the saturation point,  $(\bar{F} - \bar{F}/F_3)$ . Figure 9 verifies that the creep-force maximum is more pronounced (with an almost linear

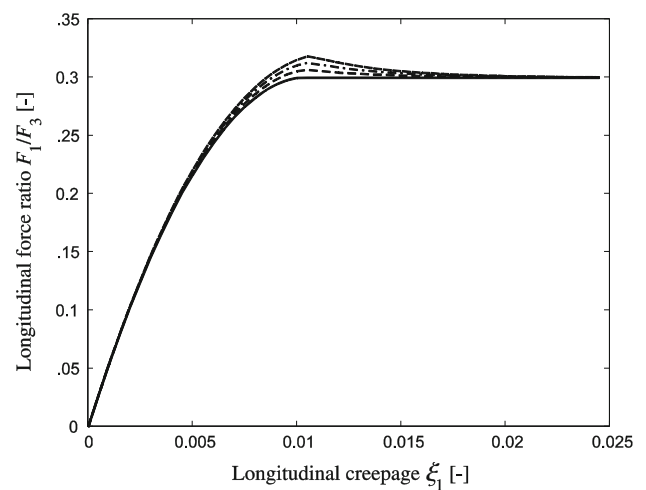


**Fig. 6** Creep-force curve setting the kinematic friction coefficient  $\mu_k = 0.30$  and increasing the static one  $\mu_s$  (*thin solid line*  $\mu_s = 0.30$ ; *dashed line*  $\mu_s = 0.35$ ; *dashed dotted line*  $\mu_s = 0.40$ ; *thick solid line*  $\mu_s = 0.45$ )

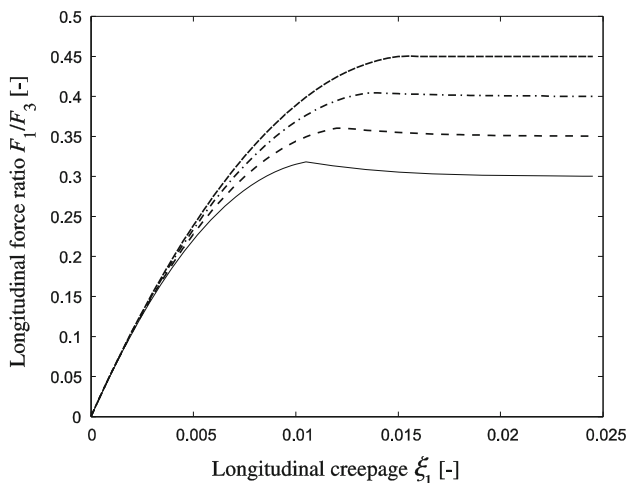


**Fig. 7** Creep–force curve setting the static friction coefficient  $\mu_s = 0.45$  and increasing the kinematic one  $\mu_k$  (*thin solid line*  $\mu_k = 0.30$ ; *dashed line*  $\mu_k = 0.35$ ; *dashed dotted line*  $\mu_k = 0.40$ ; *thick dashed line*  $\mu_k = 0.45$ )

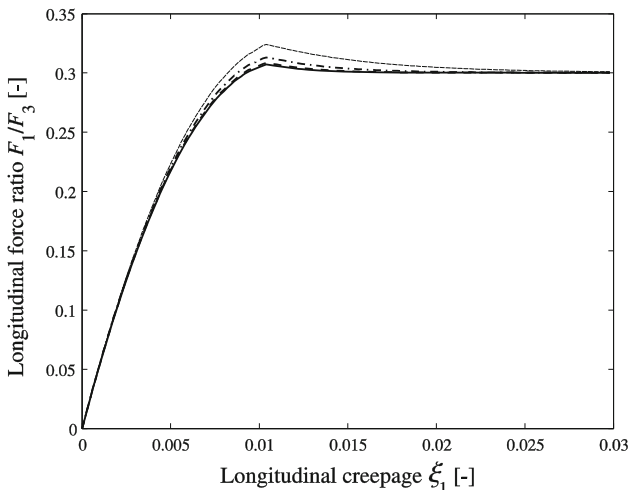


**Fig. 8** Creep–force curve setting the static friction coefficient  $\mu_s = 0.40$  and the kinematic one  $\mu_k = 0.30$  and increasing the vehicle velocity (*thin dashed line*  $V = 15$  m/s; *dashed dotted line*  $V = 25$  m/s; *thick dashed line*  $V = 35$  m/s; *thick solid line*  $V = 40$  m/s)

behaviour) compared with the saturation value when increasing  $\mu_s$ . It is interesting to point out that, for a difference about 0.15 between both coefficients ( $\mu_k = 0.35$  and  $\mu_s = 0.50$ ), normalised force difference is about 0.008 (or 6% for the relative percentage difference), while Ref. [16] showed estimations with more marked differences, about 22% for similar conditions of velocity. On the other hand, when  $\mu_k$  increases, the force peak decreases while  $\mu_k$  is approaching the fixed  $\mu_s$  coefficient, as expected (see Fig. 10); its reduction seems to be close to an exponential behaviour. Finally, Fig. 11 shows that the magnitude of the maximum is reduced similarly to that of the previous

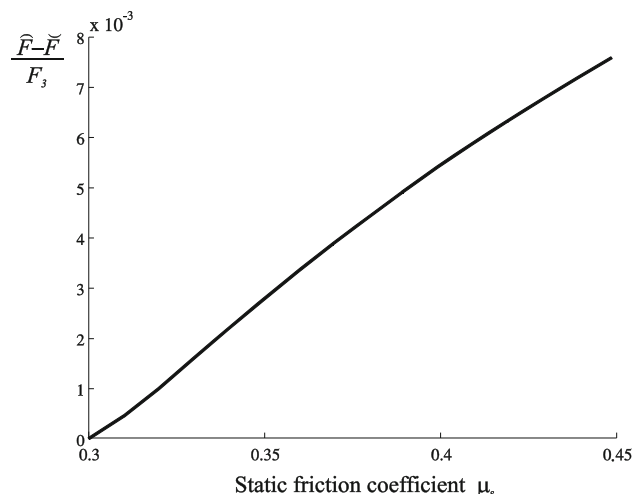


**Fig. 9** Difference between the maximum and saturation values of the creep–force setting the kinematic friction coefficient  $\mu_k = 0.35$  and increasing the static one  $\mu_s$

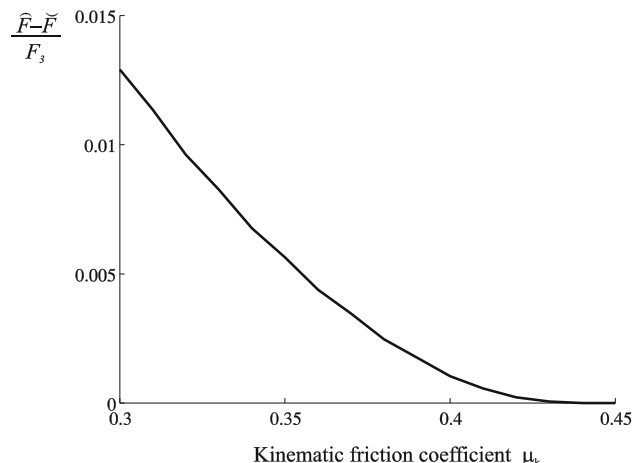


**Fig. 10** Difference between the maximum and saturation values of the creep–force setting the static friction coefficient  $\mu_s = 0.45$  and increasing the kinematic one  $\mu_k$

figure while increasing the vehicle velocity  $V$ , without varying its creepage position.

### 4.2 Comparison with Experimental Data

The tangential contact model proposed is now extended to the 3-dimensional formulation presented in Sect. 2 and compared with the measurements made in CEIT (Centre for Technical Research and Studies in San Sebastian, Spain) by using its rolling contact scaled test-bench developed in [10]. Both wheel and rail are substituted by two steel rollers. The rotational velocity of one of the rollers is 500 rpm, and the brake torque of the other is incremented with intervals of 20 N·m. This permits to

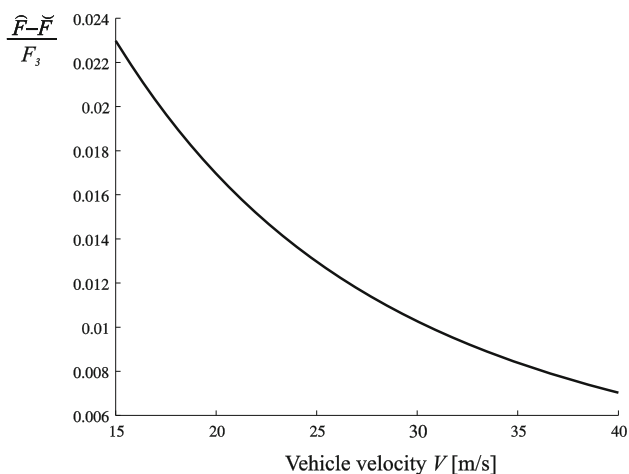


**Fig. 11** Difference between the maximum and saturation values of the creep-force setting the static friction coefficient  $\mu_s = 0.40$  and the kinematic one  $\mu_k = 0.30$  and increasing the vehicle velocity

**Table 2** Values of the test-bench for each case

Shear modulus, $G$ ( $N/m^2$ )	$8.0 \times 10^8$
Poisson's ratio, $\nu$ (-)	0.28
Roller 1 (wheel) radius, $r_{11}$ (mm)	170
Roller 1 (wheel) curvature, $r_{12}$ (mm)	300
Roller (rail) radius, $r_{22}$ (mm)	$10^6$ (flat)
Equivalent vehicle speed, $V$ (km/h)	125
Spin creepage, $\zeta_3$ ( $^\circ$ )	0

increase the longitudinal creepage while the lateral one is set for each experiment. The material and the geometrical properties for this case are detailed in Table 2.

Four different measured creep curves are presented for creepages up to 2.5%, varying the normal load (compressing both rollers) and the lateral creepage for each case. Table 3 compiles the corresponding values for each case. FASTSIM [18] software is used at this point to obtain a solution from the contact conditions detailed in Table 2. This software was developed by Kalker from its Simplified Theory in order to solve the stationary tangential contact problem with a low computational cost and an acceptable precision (with deviations around 10% from

**Table 3** Test-bench set values for each case

	Case a	Case b	Case c	Case d
Normal contact force, $F_3$ (kN)	2.0	2.1	2.3	2.3
Lateral creepage, $\zeta_2$ ( $^\circ$ )	0	0	0.025	0.120
Friction coefficient, $\mu$ (-)	0.60	0.48	0.60	0.60

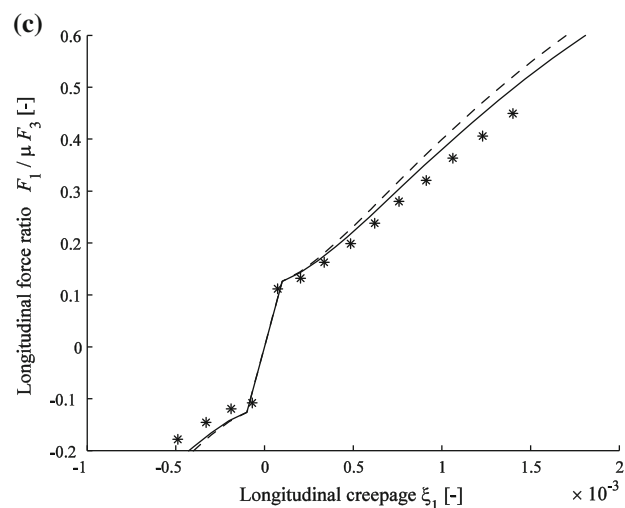
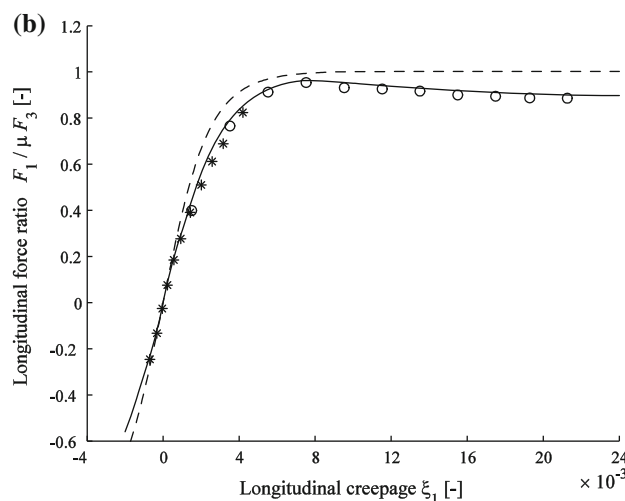
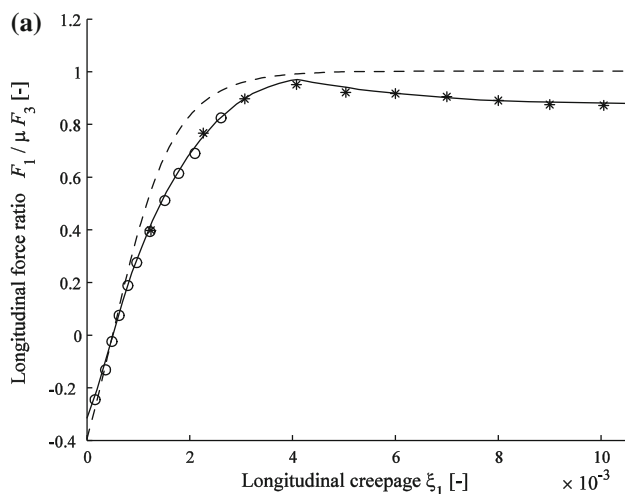


**Fig. 12** Theoretical-experimental comparison of creep-force curve (solid line numerical solution from the proposed model; dashed line FASTSIM solution; asterisk experimental set 1 from CEIT; open circle experimental set 2 from CEIT)



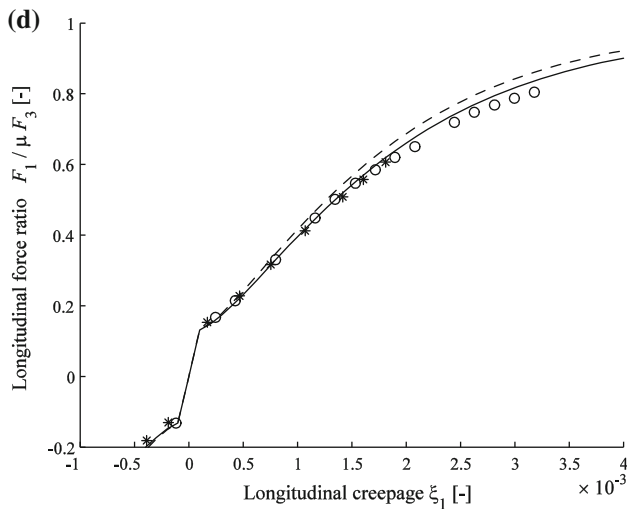


Fig. 12 continued

CONTACT if the spin is small). In this model, the displacements in a point depend exclusively on the applied tractions in that point through the flexibility coefficients (Winkler model); these flexibility coefficients were adjusted comparing them to the results given by Kalker’s Exact Theory. Results from FASTSIM and the proposed model have been plotted in Fig. 12a–d (corresponding to the cases from a to d) together with the experimental measurements.

FASTSIM solution is found from the friction coefficient  $\mu$  set in the test-bench for each case. In order to evaluate the present tangential contact model, the local parameters  $(\mu_s, \mu_k, \bar{s})$  are needed to define the local falling friction curve  $\mu(\mathbf{s})$  and hence run the tangential set of equations [Eqs. (7), (8)]. The procedure detailed in Sect. 3 is followed by detecting the characteristic points  $(\bar{F}, \bar{\xi})$  and  $(\bar{F}, \bar{\xi})$  of each experimental creep–force curve. Table 4 gathers the results obtained, which fit the measurements presented in [10].

Experimental sets in Fig. 12a, b seem to certify the non-negligible effect of the slip-dependent friction coefficient as indicated by the falling behaviour of the total tangential force after the maximal transmitted force. Hence, it suggests that the rolling contact problem cannot be modelled in a realistic way through Simplified Theories, but requires physical and Exact Theory that permits to include a variable friction coefficient. Furthermore, as mentioned

previously, Fig. 12a, b shows that experimental curves from CEIT present a less pronounced falling behaviour than creep curves for real locomotives. Together with the previous cases, in Fig. 12c, d it can be perceived how the total force measured for low creepages tends to be below the theoretical initial slope (defined by the Young’s modulus) that FASTSIM fits. It seems to indicate that falling friction reduces the effect of the static coefficient even for low creepages (when it is assumed that no percentage of the area of contact is slipping). The numerical creep curve obtained evaluating the proposed steady-state model reproduces rather well this behaviour. As seen in Fig. 12a–b, the creep curve matches the initial slope of the FASTSIM solution for low creepages, but decreases gradually adapting to the behaviour of the experimental data, even for negative creepages. The falling friction law through adopting a second coefficient  $\mu_k$  lower than  $\mu_s$  seems to reduce the initial slope of the curve compared with a single  $\mu$  curve.

Without coinciding perfectly to the experimental set, location and magnitude of the maximum matches notably well for Fig. 12a, b, indicating that the previous procedure seems to be valid for relating both global and local curves. Finally, the curve is forced to match the saturation value for higher creepages through the kinematic coefficient estimated, showing hence that the difference between both maximum and saturation value is not strongly pronounced.

### 5 Conclusions

In this work, a method for introducing a falling friction coefficient in rolling contact mechanics is presented. This method is suitable for creepages that slightly exceed the saturation conditions (lower than 3% if the solids in contact are made of steel), which correspond to the creepage range in most of the railway dynamic studies. The technique adopts steady-state conditions, and the friction coefficient is a function of the local slip velocity through a simplified Stribeck curve.

The formulation is based on Kalker’s Variational Theory, which adopts the non-steady-state hypotheses. All the same, the literature shows that Variational Theory produces peaks in the contact traction distribution when two friction coefficients are implemented. The present approach

Table 4 Parameters of the falling friction coefficient curve

	Case a	Case b	Case c	Case d
Static friction coefficient, $\mu_s$ (-)	0.60	0.49	0.61	0.60
Kinematic friction coefficient, $\mu_k$ (-)	0.62	0.45	0.58	0.57
Local slip saturation value, $\bar{s}$ (m/s)	0.51	0.41	0.46	0.47

modifies the original method by means of the regularisation of the Coulomb's law, which eliminates the presence of such peaks. An additional advantage of the implementation of the regularisation is a significant reduction of the computational costs when compared to the original method thanks to the saving in the number of equation unknowns.

The implementation of the velocity-dependent friction coefficient adds new variables that frequently have been chosen unrealistically in the literature. The present work develops the constrain equations that establish mathematical relationships between the different parameters associated with the falling friction rolling contact problem. These constrain equations facilitate to build models that produce realistic results from experimental data. In this respect, the proposed model reasonably fits the experimental creepage versus creep-force curves obtained from high-precision test-bench measurements.

The appearance of the creepage versus creep-force curves obtained from the proposed methodology does not differ markedly from the one of a single friction coefficient. This conclusion is in accordance with previous test-bench measurements that present a slight decrease in the tangential force once the maximum is reached.

A global model that fits all the creepage range level is to the authors' best knowledge, undone. By considering the negligible role of the displacements due to the elastic deformation in high creepage conditions, the present model can be adequate in traction locomotive problems if a suitable Stribeck curve is adopted. In such case, the above-presented constrain equations associated with the parameter set have to be reconsidered.

**Acknowledgements** The authors acknowledge the financial contribution of the Spanish Ministry of Economy and Competitiveness through the Project TRA2013-45596-C2-1-R.

**Open Access** This article is distributed under the terms of the Creative Commons Attribution 4.0 International License (<http://creativecommons.org/licenses/by/4.0/>), which permits unrestricted use, distribution, and reproduction in any medium, provided you give appropriate credit to the original author(s) and the source, provide a link to the Creative Commons license, and indicate if changes were made.

## References

- Grassie, S.L., Elkins, J.A.: Rail corrugation on North American transit systems. *Veh. Syst. Dyn.* **28**, 5–17 (1998)
- Hsu, S.S., Huang, Z., Iwnicki, S.D., Thompson, D.J., Jones, C.J.C., Xie, G., Allen, P.D.: Experimental and theoretical investigation of railway wheel squeal. *Proc. Inst. Mech. Eng. F J. Rail Rapid Transit* **221**, 59–73 (2007)
- Kalker, J.J.: *Three-Dimensional Elastic Bodies in Rolling Contact*. Kluwer, Dordrecht (1990)
- Polach, O.: Influence of locomotive tractive effort on the forces between wheel and rail. *Veh. Syst. Dyn.* **35**, 7–22 (2001)
- Giménez, J.G., Alonso, A., Gómez, E.: Introduction of a friction coefficient dependent on the slip in the FastSim algorithm. *Veh. Syst. Dyn.* **43**, 233–244 (2005)
- Baeza, L., Vila, P., Roda, A., Fayos, J.: Prediction of corrugation in rails using a non-stationary wheel-rail contact model. *Wear* **265**, 1156–1162 (2008)
- Vollebregt, E.A.H., Schuttelaars, H.M.: Quasi-static analysis of two-dimensional rolling contact with slip-velocity dependent friction. *J. Sound Vib.* **331**, 2141–2155 (2012)
- Avlonitis, M., Kalaitzidou, K., Streator, J.: Investigation of friction statics and real contact area by means a modified OFC model. *Tribol. Int.* **69**, 168–175 (2014)
- Berger, E.J., Mackin, T.J.: On the walking stick-slip problem. *Tribol. Int.* **75**, 51–60 (2014)
- Alonso, A., Guiral, A., Baeza, B., Iwnicki, S.D.: Wheel-rail contact: experimental study of the creep forces-creepage relationships. *Veh. Syst. Dyn.* **52**(S1), 469–487 (2014)
- Spiryagin, M., Polach, O., Cole, C.: Creep force modelling for rail traction vehicles based on the Fastsim algorithm. *Veh. Syst. Dyn.* **51**, 1765–1783 (2013)
- Vollebregt, E.A.H.: Numerical modeling of measured railway creep versus creep-force curves with CONTACT. *Wear* **314**, 87–95 (2014)
- Kalker, J.J.: *On the Rolling Contact of Two Elastic Bodies in the Presence of Dry Friction*. PhD Thesis, Technical University of Delft (Holland) (1967)
- Baeza, L., Fuenmayor, F.J., Carballeira, J., Roda, A.: Influence of the wheel-rail contact instationary process on contact parameters. *J. Strain Anal. Eng.* **42**, 377–387 (2007)
- Le Rouzic, J., Le Bot, A., Perret-Liaudet, J., Guibert, M., Rusanov, A., Douminge, L., Bretagnol, F., Mazuyer, D.: Friction-induced vibration by Stribeck's law: application to wiper blade squeal noise. *Tribol. Lett.* **49**, 563–572 (2013)
- Rabinowicz, E.: The nature of the static and kinetic coefficients of friction. *J. Appl. Phys.* **22**, 1373–1379 (1951)
- Carter, F.W.: On the action of locomotive driving wheel. *Proc. R. Soc. Lon. Ser. A* **112**, 151–157 (1926)
- Kalker, J.J.: A fast algorithm for the simplified theory of rolling contact. *Veh. Syst. Dyn.* **11**, 1–13 (1982)